

MINERALOGICAL CHARACTERISTICS AND MICROMORPHOLOGICAL OBSERVATIONS OF BRITTLE/SOFT Fe/Mn CONCRETIONS FROM OKINAWAN SOILS

L. P. VIDHANA ARACHCHI¹, Y. TOKASHIKI^{2,*} AND S. BABA²

¹ Coconut Research Institute, Lunuwila, Sri Lanka

² Department of Environmental Science and Technology, Faculty of Agriculture, University of the Ryukyus, Nishihara-cho, Okinawa 903 0213, Japan

Abstract—Manganese minerals are not common and the distinction of poorly crystalline Mn minerals from other associated minerals is important. For many years, the crystal structures of poorly crystalline Mn minerals in Fe/Mn concretions have been the subject of considerable conjecture and controversy. This study reports the micromorphological and mineralogical characteristics, and the chemical composition of Fe/Mn minerals in soft Fe/Mn concretions formed in Shimajiri Mahji soils (Typic Hapludalfs) that developed from Ryukyu limestone on Okinawa Island, Japan. The Fe/Mn minerals in brittle/soft Fe/Mn concretions were characterized using a sequential selective dissolution procedure (SSDP) by treatments with NaOH, hydroxylamine hydrochloride (HAHC) at 25°C and 60°C, and dithionite-citrate-bicarbonate (DCB) in combination with X-ray diffraction (XRD) and scanning electron microscopy (SEM). The HAHC treatment at 25°C dissolved birnessite, but not lithiophorite and goethite. A subsequent extraction with HAHC at 60°C dissolved lithiophorite but not goethite. Finally, the DCB treatment was able to dissolve goethite. The SEM images show that birnessite crystals, with a blade- or plate-like habit, form globular aggregates inside veins and cavities. Pseudo-hexagonal crystals of lithiophorite have produced thread-ball structures with crystal shape similar to birnessite and birnessite crystals are closely associated with lithiophorite. Well developed hexagonal plates of gibbsite crystals are clustered in different directions to make foliated vermiciform structures. Aggregates of goethite crystals are acicular and are arranged into stars. The supplementary SSDP, in combination with XRD and SEM techniques, provides methods to distinguish and partly quantify birnessite and lithiophorite in the presence of layer silicate and Fe oxide minerals and confirm their own morphological features.

Key Words—Chemical Composition, Fe/Mn Minerals, Layer Silicate, Mineral Micromorphology, SEM and XRD Techniques, Sequential Selective Dissolution Procedure

INTRODUCTION

Iron-manganese nodules have been found in many soils, particularly those which are poorly drained or have some internal drainage restrictions. Manganese minerals occur as fine-grained aggregates or veins, as marine and fresh-water nodules and concretions, and as crusts and coatings on other mineral particles and rock surfaces. Birnessite is one of the Mn minerals which occurs as coatings on other soil particles, as concretions in cracks and veins, and mixed with Fe oxides and other soil constituents in nodules (McKenzie, 1989). However, Mn minerals typically occur as fine-grained mixtures, making it difficult to study their micromorphology and crystal chemistry (Post, 1999).

The usually large adsorption capacities and scavenging properties of Mn oxide/hydroxide minerals provide one of the primary controls of heavy metals and other trace elements in soil and aquatic sediments. Birnessite group minerals, in particular, belong to the phyllosilicate minerals, have layered structures, readily undergo

oxidation/reduction and cation-exchange reactions, play a major role in controlling groundwater chemistry, and both biological and non-biological oxidation probably contribute to the formation of birnessite in soils (Post, 1999). Understanding such controls through characterization and elemental composition of Fe/Mn minerals is important for maintaining and improving the fertility of soil, mitigating health effects in humans and animals, and for treatment of water for consumption and industrial use. On the other hand, Mn oxides (*viz.* birnessite, todorokite and lithiophorite) are important oxidants in soil. They have been the focus of much recent research because they are major oxidants of Cr(III) to the more toxic Cr(VI) form (Dixon, 2002; Fendorf and Zasoski, 1992).

Poorly crystalline varieties of Mn oxides in soils have been identified on a number of occasions (White and Dixon, 1986; McKenzie, 1989; McDaniel and Buol, 1991). The most intense and significant diffraction maxima of illite/mica and kaolinite coincide with the diffraction maxima of Mn minerals (Min Zhang and Karathanasis, 1997). The 001 XRD peak of kaolinite often obscures the 0.725 nm peak of birnessite (Ross *et al.*, 1976; McKenzie, 1989). Therefore, reliable methods

* E-mail address of corresponding author:
toka2841@agr.u-ryukyu.ac.jp
DOI: 10.1346/CCMN.2004.0520407

for distinguishing Mn minerals from other Fe oxide and silicate minerals are rare. Chao (1972) utilized acidified hydroxylamine hydrochloride to dissolve Mn oxides from soils and sediments. This simple step was useful for dissolving Mn and Fe oxides, separately and for determining the respective metal ions that were released. Tokashiki *et al.* (1986) and Golden *et al.* (1993) combined selective dissolution procedures with XRD analysis. In their studies, concentrated NaOH was used to dissolve kaolin minerals and hydroxylamine hydrochloride was used to distinguish birnessite from Fe oxides. Tokashiki *et al.* (2003), also used various steps of a SSDP to separate birnessite and lithiophorite from Fe oxides in hard Fe/Mn nodules from soils. X-ray diffraction alone does not indicate either the crystal morphology or the mode of occurrence of these minerals within the Fe/Mn nodules or concretions. Therefore, the present study combines different steps of SSDP with XRD and SEM analysis to distinguish Mn minerals from Fe and other silicate minerals. In addition, the study also evaluates the effectiveness of the conditions of each step of SSDP to dissolve individual Fe/Mn minerals using XRD and SEM techniques. Observations during the successive steps of SSDPs confirmed the micromorphological structures of Fe/Mn minerals in brittle/soft Fe/Mn concretions from Okinawan soils.

It is important to document the detailed micromorphology of Fe/Mn minerals and their associated minerals such as kaolinite, gibbsite and illite minerals for different soils in order to understand weathering processes and chemical reactions in their environment. However, detailed information on the micromorphology of natural lithiophorite, birnessite and their relationships are rare. There is a lack of detailed information on Mn minerals in brittle Fe/Mn concretions in imperfectly drained soil which originated from limestone in Okinawa, Japan.

This study was conducted to: (1) examine the micromorphology of Fe/Mn minerals and their associated minerals in Fe/Mn-rich brittle concretions using SEM; (2) determine the chemical and mineral composition of Fe/Mn-rich brittle concretions; and (3) evaluate the effectiveness of sequential selective dissolution treatments for identification of micromorphology of Fe/Mn minerals in brittle/soft concretions.

MATERIALS AND METHODS

Experimental site

The study area near Okinawa City, Japan, is characterized by a hilly or rolling topography of moderate relief, with elevation ranging from ~35 to 50 m above sea level. Samples were collected from a hilly area covered with *Imperata cylindrical Beauv.* Var. (Chigaya) and with *Pinus luchensis Mayr* (Ryukyu Matsu). The mean annual temperature is ~22°C, and the mean temperatures in the coldest month (January)

and hottest month (July) are 5.4°C and 34.5°C, respectively. The mean annual rainfall is ~2680 mm, with a maximum of 3982 mm in 1969, and a minimum of 1905 mm in 1977. Typhoons occur frequently between July and October, bringing high rainfall and strong winds to the island. The soil is classified as a Shimajiri Majhi soil, which belongs to the Calcaric Dark Red sub group (Udalfs; according to the USDA Soil classification). The soil profile at the experimental site showed three distinct soil horizons, namely, A (0–5 cm), B1 (5–50 cm) and B2 (>50 cm). The soil is imperfectly drained due to the presence of a clay pan (below 150 cm depth) in the sub-soil. Black soft/brittle Fe/Mn concretions are deposited as a layer (~5 cm thick) within the B2t horizon (100–115 cm). Samples from these Fe/Mn concretions were collected for detailed micromorphological, mineralogical and chemical analysis. The bedrock is composed mainly of limestone (Tokashiki *et al.*, 1986). The mean bulk density of Shimajiri Majhi soil is $1.21 \pm 0.06 \text{ Mg/m}^3$ and the mean percentage of coarse sand, fine sand, silt and clay are $3.7 \pm 0.8\%$, $12.4 \pm 1.9\%$, $29.2 \pm 5.1\%$ and $54.6 \pm 7.3\%$, respectively. This soil covers ~41% of Okinawa and is classified as a moderately productive soil, due to poor physical characteristics in the sub-horizons.

Minerals and elemental analysis

About 100 samples (1 cm in diameter) of Fe/Mn brittle/soft concretions were ground in distilled water using an agate mortar and pestle. Clay fractions of the ground Fe/Mn brittle/soft concretions were separated by sedimentation (Jackson, 1969) and the clay fraction was adjusted to the concentration of 5 g/L of suspension. Sequential selective dissolutions were carried out on the <2.0 µm fraction of two sets of samples using the method proposed by Tokashiki *et al.* (1986, 2003) (Figure 1). This method is summarized as follows: (1) 10 mL (50 mg) of suspension were placed in each of five 10 mL teflon centrifuge tubes and centrifuged for 10 min at $1500 \times g$ to separate the clay fractions, and the initial supernatant liquids from five tubes were decanted. The 5th tube was separated as a control (untreated clay residues). (2) 10 mL of 5 M NaOH were added to each of four centrifuge tubes that were mixed by sonication for 10 s, and placed in a water bath for 60 min at 90–95°C to dissolve kaolinite and gibbsite. Samples were allowed to cool to room temperature and centrifuged for 10 min at $1500 \times g$. After sonication for 10 s, residues were washed with 8 mL of distilled water to remove excess base and residue in the 4th tube to be used for NaOH treatment. (3) 10 mL of 0.1 M hydroxylamine hydrochloride (0.1 M HAHC) were added to three tubes, mixed by sonication for 10 s, and shaken at 25°C for 10 min to dissolve birnessite, and centrifuged for 10 min at $1500 \times g$. The residue in the 3rd tube was separated using a 0.1 M HAHC (25°C) treatment. (4) The residues in the remaining two tubes were again

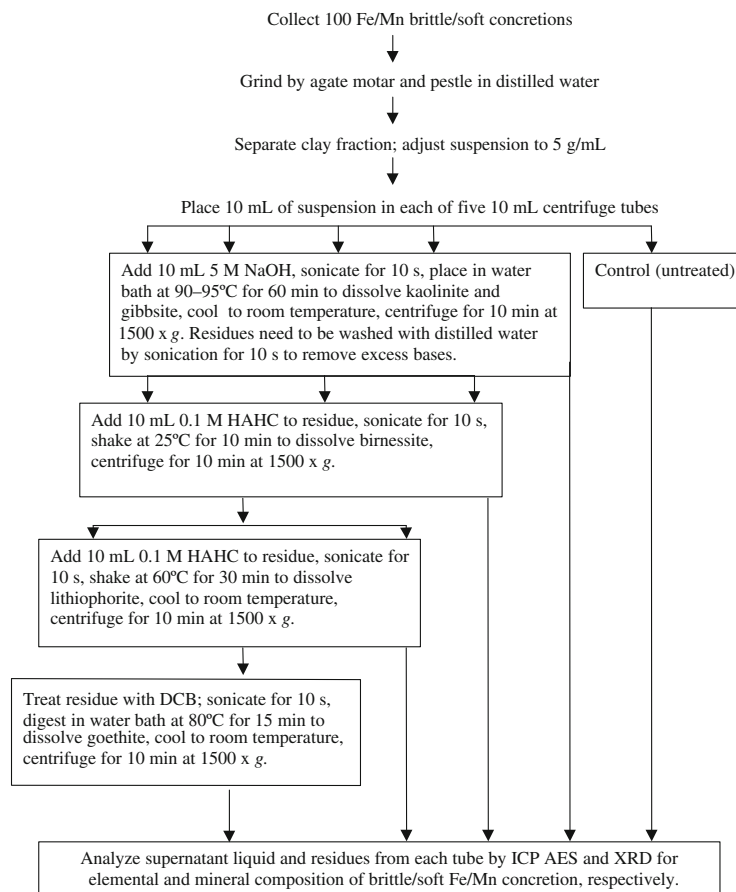


Figure 1. Flow diagram for sequential selective dissolution procedure (SSDP).

treated with 10 mL of 0.1 M HAHC at 60°C for 30 min to dissolve lithiophorite. These two tubes were then allowed to cool to room temperature, were centrifuged, and the 2nd tube was separated as a 0.1 M HAHC (60°C) treated residue. (5) The last sample was treated with DCB and sonicated for 10 s and placed in a water bath for 15 min at 80°C to dissolve goethite as proposed by Mehra and Jackson (1960), and considered as a DCB-treated sample. The supernatant liquids for each step were analyzed by inductively coupled plasma atomic emission spectrometry (ICP-AES).

Residues from the steps above were mounted on a glass slide, air dried, and analyzed by XRD from 2 to 30°2θ using CuKα radiation at 30 kV and 10 mA with a scanning speed of 0.5°/min. Another 10 mL (50 mg) of suspension were centrifuged to separate the clay fraction, treated with DCB only (without NaOH), and analyzed by XRD using the conditions above with a scanning speed of 1°/min after Mg and K saturation. The K-saturated, air-dried clay samples were analyzed after progressive heating at 105°C, 300°C and 550°C. The Mg-saturated clays were analyzed when air dried and after glycerol solvation.

Scanning electron microscope study

The Fe-/Mn-rich brittle/soft concretions were broken into small pieces (1 cm in diameter). De-ionized water was sprayed on the broken pieces to wash off any adhering debris. The Fe/Mn concretions were then crushed into small pieces in an agate mortar and air dried. About 100 black pieces (2–5 mm) were hand-picked randomly. The prepared specimens were dried by heating at 105°C for 24 h, then stored in a desiccator. Some of these pieces were mounted on carbon-coated brass stubs for SEM analysis. Finally, the specimens were sputter coated with gold (20 nm thick) and analyzed under high vacuum (HV) by SEM (JEOL-JSM-5600 LV, Japan) equipped with a back-scattered electron detector as described by Davey (1978).

Micromorphology of residues of the sequential selective dissolution procedure (SSDP)

Using SEM we examined the effect of the various SSDP treatments on the Fe/Mn minerals. Preliminary studies showed that when the clay fraction was ultrasonicated for 10 s, specific morphological features of minerals were disturbed. Therefore, silt and clay

fractions of Fe/Mn residues were reacted with the various SSDP reagents (Figure 1) without ultrasonication.

The treated residues were oven dried (105°C), stored in a desiccator, mounted on carbon-coated brass stubs, coated with gold, and analyzed by SEM as described above. More than 50 samples were examined and numerous representative photomicrographs were taken.

RESULTS AND DISCUSSION

Characterization of Fe/Mn minerals and their elemental composition

The XRD patterns of the untreated clay fraction exhibited a series of peaks at 1.42, 1.0, 0.945, 0.725, 0.485, 0.472, 0.418, 0.357 and 0.334 nm (Figure 2). A peak appeared at 1.4 nm in Mg- and K-saturated samples and showed a gradual reduction of peak intensity. It shifted to 1.0 nm on heating, representing a vermiculite-mica and hydroxy-interlayered vermiculite (Figure 3). The peaks at 0.725 nm are due to kaolinite with a possible contribution from birnessite (Figure 2). The peaks that appeared at 1.0, 0.50 and 0.334 nm represent illite (Figure 3). Peaks that appeared at (0.945, 0.472), 0.485 and 0.418 were due to lithiophorite, gibbsite and goethite, respectively (Figure 2A,B,C). The 5 M NaOH treatment at 95°C dissolved the kaolinite and gibbsite, allowing XRD peaks for lithiophorite (0.945, 0.472 nm)

Table 1. Extractable Fe, Mn, Al and Si in each extract (g kg⁻¹) from the successive dissolution procedure.

Reagent	Fe	Mn	Al	Si
NaOH	0	0	137±6.8 (14%)	67.0±2.3 (7%)
HAHC (25°C)	3.6±0.6 (0.4%)	39.0±1.4 (4%)	0	0
HAHC (60°C)	3.0±0.5 (0.3%)	2.0±0.2 (0.2%)	0	0
DCB	90.0±3.1 (9%)	0	5.4±1.1 (0.5%)	1.9±0.2 (0.2%)
Total	96.6	41.0	142.4	68.9

±: standard deviation

and birnessite (0.725 nm) to be observed. The results of the elemental analysis of extracts for each step of SSDP (Table 1) indicate high Al and Si concentrations. Aluminum and Si concentrations were greater in the NaOH extracts, consistent with the dissolution of kaolinite and gibbsite. The high intensity of the XRD peak of gibbsite may be due to its high concentration in brittle Fe/Mn sediments (Figures 3, 5A,B). The 5 M NaOH treatment followed by the 0.1 M HAHC at 25°C

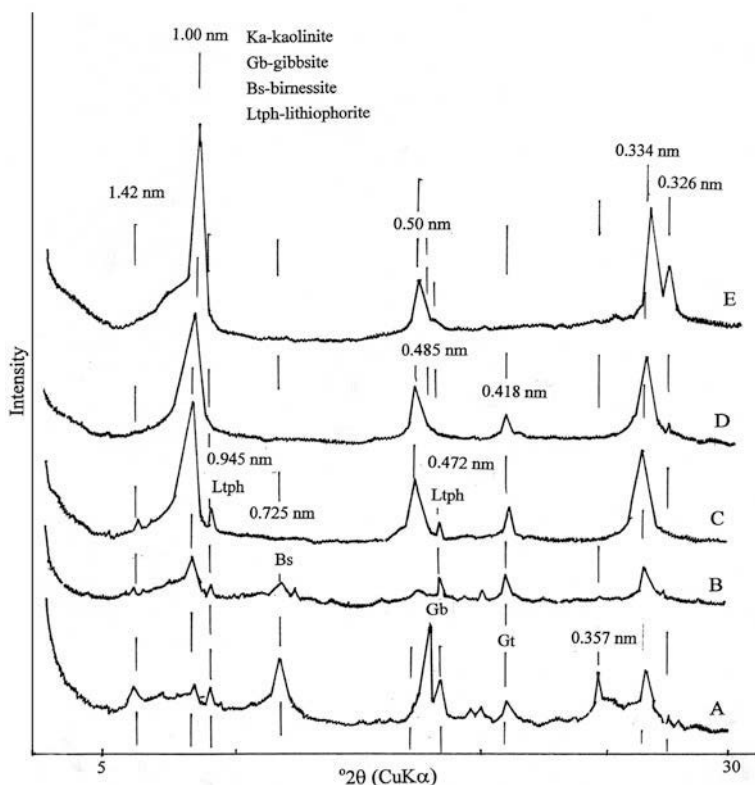


Figure 2. XRD patterns of a brittle/soft Fe/Mn sample (<2 μm clay fraction) treated by sequential selective dissolution with NaOH treatment. (A) Untreated, (B) NaOH, (C) NaOH + HAHC (25°C), (D) NaOH + HAHC (60°C), (E) NaOH + HAHC (60°C) + DCB.

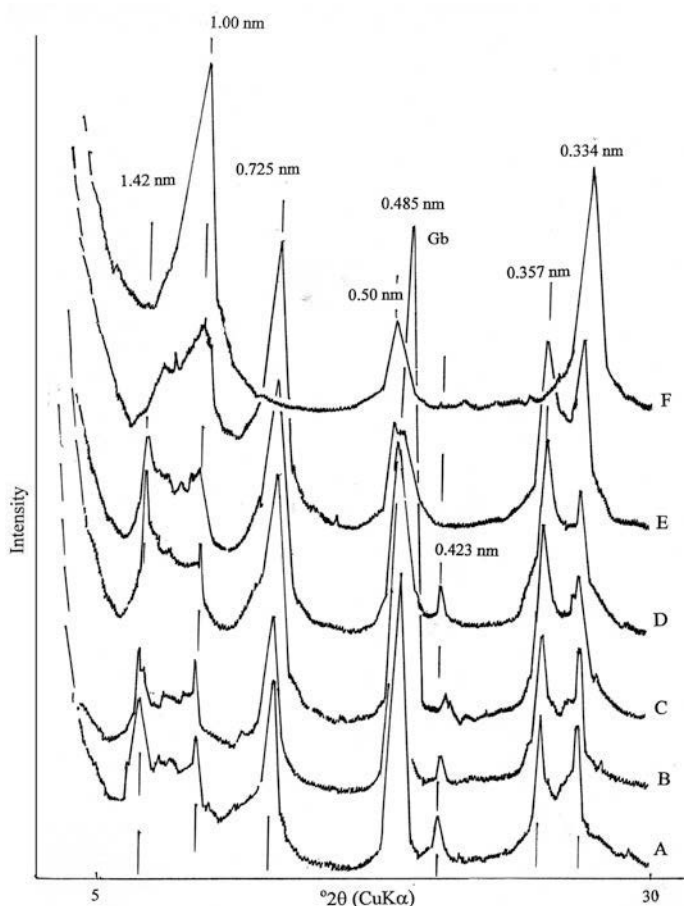


Figure 3. XRD patterns of brittle/soft Fe/Mn sample ($<2 \mu\text{m}$ clay fraction) treated with DCB without NaOH treatment. (A) Mg-clay (air-dried), (B) Mg-clay (glycerol saturation), (C) K-clay (air-dried), (D) K-clay (105°C), (E) K-clay (300°C), (F) K-clay (550°C).

resulted in a decrease of the birnessite peaks (0.725 nm), while the lithiophorite peaks (0.945, 0.472 nm) and goethite peak (0.418 nm) remained (Figure 2C). Subsequently, the lithiophorite peaks (0.945, 0.472 nm) decreased following treatments with HAHC at 60°C for 30 min, while the goethite peak remained (Figure 2D). The highest level of Mn (39 g/kg) and Fe (90 g/kg) were in the extracts of HAHC (25°C) and DCB treatment, respectively (Table 1). The Mn extracted by the HAHC (25°C) treatment was primarily associated with birnessite as confirmed by the disappearance of the birnessite 0.725 nm XRD peak (Figure 2C). The amount of Mn extracted by the HAHC (60°C) was less than that of HAHC (25°C), indicating the presence of a small amount of lithiophorite (Ltpb) in brittle/soft Fe/Mn concretions. The presence of lithiophorite in natural soil is negligible (McKenzie, 1989) and the $<2 \mu\text{m}$ clay fraction used in this study might also be the one of reasons for the small amount of lithiophorite. However, both XRD and SEM analysis confirm the presence of lithiophorite in soft/brittle Fe/Mn concretions in Okinawa Island (Figures 2 and 4d). The high Mn concentration (39 g/kg) in HAHC (25°C) extract was due to complete dissolution of

birnessite (Table 1). The 0.418 nm goethite peak disappeared following DCB treatment (Figure 2E). Most of the DCB-extractable Fe was due to the presence of goethite. A small amount of Al (5.4 g/kg) and Si (1.9 g/kg) in the DCB extract might have been released from amorphous silicate minerals or goethite (Table 1). The total amounts of Fe, Mn, Si and Al elements in Fe/Mn platy sediments are 96.6, 41, 142.4 and 68.9 g/kg, respectively

The XRD and chemical analysis indicate that the SSDP was useful for identifying and selectively dissolving Fe/Mn oxides. The major mineral constituents identified in the brittle Fe/Mn concretions were vermiculite-mica and hydroxy interlayered vermiculite minerals, illite, kaolinite, birnessite, gibbsite, lithiophorite and goethite.

Micromorphology of Fe/Mn and their associated minerals

Manganese oxide minerals: birnessite. The occurrence of birnessite in Fe-Mn nodules is difficult to determine (McKenzie, 1989). However, birnessite was found in most of the Fe/Mn concretions from the Shimajiri Mahjii

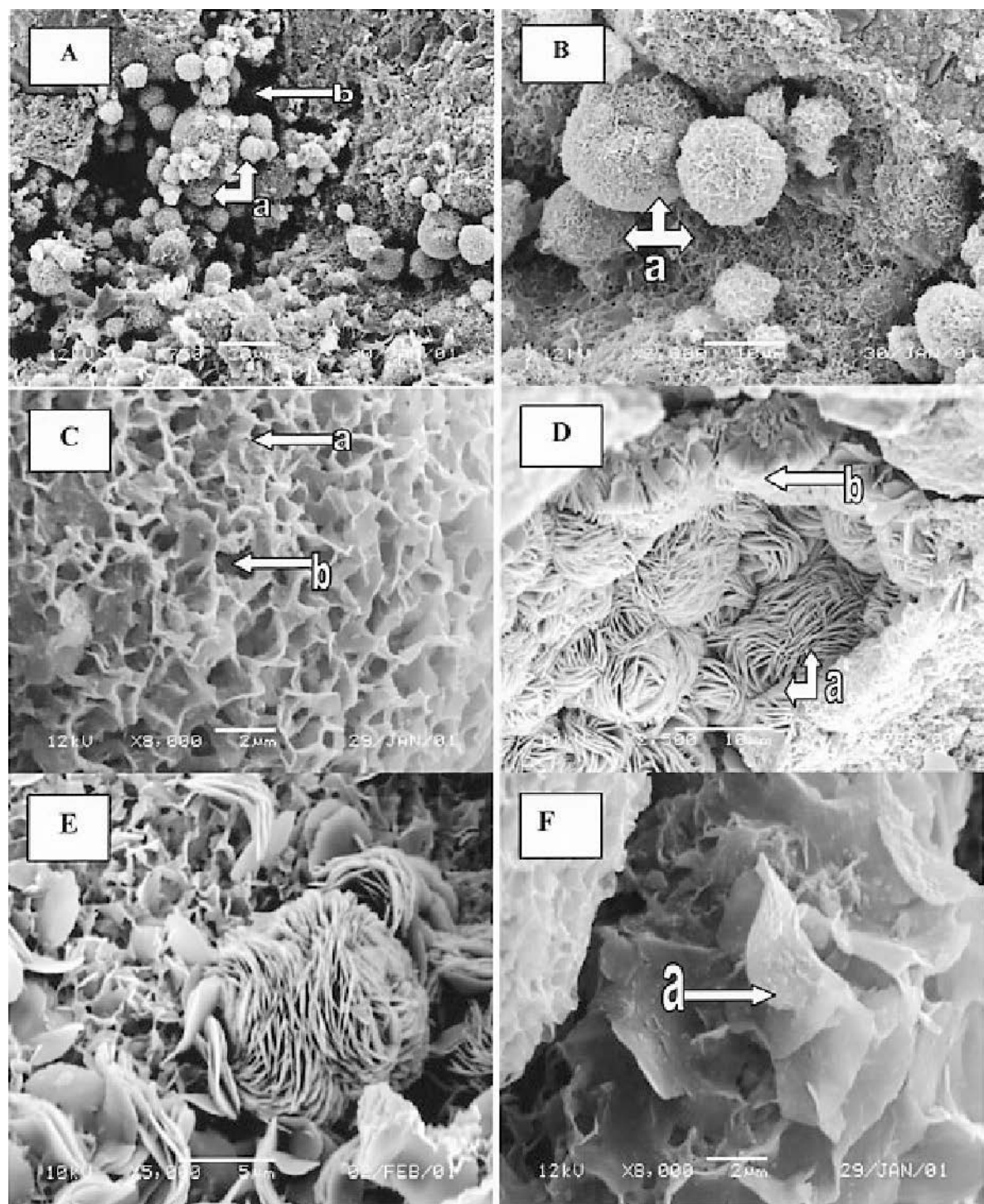


Figure 4. SEM images of brittle Fe/Mn concretions showing the micromorphology and occurrence of Mn oxide and illite minerals. (A) Occurrence of globular aggregates of birnessite (A-a and B-a) in the cavities (A-b); (B) the unusual variation of crystal arrangements represents the poor crystallinity and amorphous nature of birnessite; (C) poorly developed crystals of birnessite (C-a) produce many cavities (C-b); (D) aggregation of lithiophorite crystals to produce thread-ball structures (D-a); (E) association of lithiophorite with birnessite and their uneven crystal edges (D-b); (F) orientation of illite crystals.

soils. Ross *et al.* (1976) identified birnessite from acidic horizons of Udult Suborders. The micromorphology and

concretionary pattern of birnessite are illustrated in Figure 4A,B,C. Different sizes of honeycomb morphol-

ogies of birnessite (Figure 4A-a,B) are aggregated and deposited inside cavities (Figure 4A-b) and veins of Fe/Mn concretions. Birnessite with similar crystal shape and kind of aggregation was found in sea sediments near Hokkaido, Japan (Usui and Mita, 1995). The detailed morphology of surface of globe-shaped structures of birnessite shows that birnessite crystals have a blade/plate-like habit (Figure 4C-b). The surface of the aggregates of birnessite produces several cavities and edges of birnessite plates. Few studies have (Burns and Burns, 1977; Lonsdale *et al.*, 1980) have documented the morphology of natural birnessite as was achieved here, formed in seawater-based hydrothermal fluids. Uzochukwu and Dixon (1986) found birnessite and lithiophorite in the nodules formed by the leaching of Mn from acid upper horizons followed by Mn precipitation in the neutral to alkaline subsoil. However, there are no reports of birnessite formed in imperfectly drained soils in tropical environments. On the other hand, the cavity arrangement of honeycomb crystallization also illustrates that birnessite consists of radiating rods as described by Burns and Burns (1977) and Lonsdale *et al.* (1980). Golden *et al.* (1988) also observed the platy micromorphology of synthetic birnessite. The typical rapid, special variation of irregular platy crystal sizes, shape of aggregation (Figure 4C), and low peak intensities (Figure 2) explain the poor crystallinity of birnessite. Its radiating platy structure suggests that globular masses of Mn oxide crystallized very rapidly (Lonsdale *et al.*, 1980). Post (1999) reported that Mn oxide minerals commonly occur as coatings and fine-grained aggregates with large surface areas, exerting chemical influences far out of proportion to their concentrations.

Mn oxide minerals: lithiophorite. The crystal shape of synthetic lithiophorite was reported to be hexagonal by McKenzie (1989), but his photomicrographs suggest that synthetic lithiophorite forms pseudohexagons. Yang and Wang (2003) successfully prepared lithiophorite under highly alkaline conditions and the shape of the synthetic lithiophorite crystals was pseudohexagonal. The morphology of well developed natural lithiophorite is shown in Figure 4D,E. Pseudohexagonally shaped plates of natural lithiophorite crystals are arranged radially and have produced compacted thread-ball structures (Figure 4D-a). Similar to our observations, other researchers (*e.g.* Paulings and Barclay, 1982; Post and Appleman, 1994; Barbara *et al.*, 1993) also observed that the clustered, pseudohexagonally shaped crystals of lithiophorite occurred as compacted ball structures. The many micro-cavities/veins between lithiophorite plates increase the surface area of the lithiophorite minerals. Those crystals are also closely associated with birnessite (Figure 4E). The shapes of the peaks of lithiophorite and birnessite in XRD charts (Figure 2A,B,C) and SEM images (Figure 4A,B,C,D)

demonstrate that lithiophorite is more crystallized than birnessite

Fe oxide minerals: goethite. Goethite is one of the most common Fe oxides in soils and the crystals are usually sub-micron in size and frequently have well developed crystal faces (Dixon, 1999). The micromorphology of the goethite mineral is shown in Figure 5E. Aggregates of acicular goethite crystals are arranged into stars (Figure 5E-a). The detailed morphology of goethite also shows that the shape of individual goethite crystals is grass-leaf like and these acicular goethite particles are rare (Schwertmann and Kampf, 1988), but typically form in poorly drained soils (Schwertmann and Taylor, 1989). Goethite particles produced in the presence of high Al concentrations in Fe/Mn concretions are more equidimensional and do not orient well (Ford *et al.*, 1997).

Complementary to our study, a similar micromorphology of natural goethite was reported by Schwertmann and Taylor (1989). The crystal shape of synthetic goethite in alkaline conditions is usually acicular and often consists of several domains within the crystal along the needle axis (Schwertmann and Taylor, 1989; Ford *et al.*, 1997).

Al hydroxide minerals: gibbsite. PSEM images and XRD analysis illustrate a high concentration of gibbsite in our samples (Figures 3A, 5A,B). Well developed (Figure 5B-a) hexagonal gibbsite plates are clustered systematically in different directions to make foliated vermiciform structures. The micromorphology of natural and industrial gibbsite crystals is usually reported as pseudohexagonal plate-like with {001} basal and {001} and {110} side edges (Eswaran *et al.*, 1977; Hsu, 1989; Sweegers *et al.*, 1999; Sean *et al.*, 2000). However, well developed flattened hexagonal crystals were built up into six domains where, in each crystal domain, either the *a* or *b* axis is perpendicular to the side faces (Figure 5B-a). Those structures suggest a ‘card-house’ aggregation of flat plates against a sharp edge, resulting in a lot of void space in the aggregate (Figure 5B-a,C-a). The crystal shape of gibbsite and its orientation in soft/brittle Fe/Mn concretions from imperfectly drained soil of Okinawa, resembles that found by Sweegers *et al.* (1999), and Peskleway *et al.* (2003). They also reported flattened crystals. The photomicrographs also clearly show well developed hexagonal platy gibbsite crystals (Figure 5C-b) randomly arranged on the surface of the globular structures of birnessite (Figure 5D-a) leaving voids among gibbsite crystals which sometimes associate with irregularly shaped kaolinite crystals (Figure 6B). Eswaran *et al.* (1977) also found that, in a lateritic soil from Zaïre, gibbsite occurs on argillans, in randomly oriented crystal sheets, as nodular aggregates infilling vugs and on ped faces. In absolute accumulation, the gibbsite crystallizes in voids in the soil material indicating that there was a possibility of Al transport in

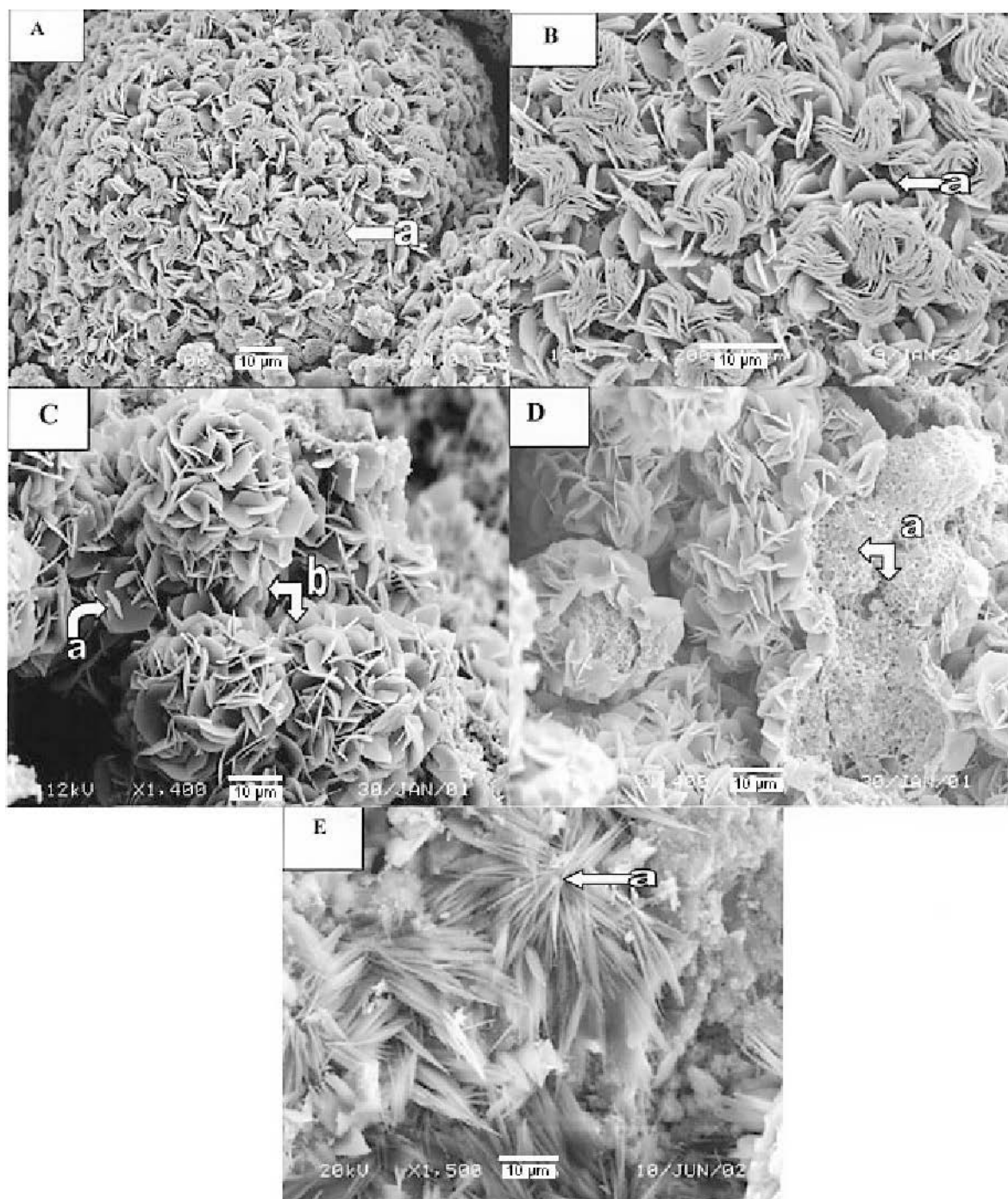


Figure 5. SEM images of brittle Fe/Mn concretions showing the micromorphology and occurrence of Al and Fe oxide minerals. (A) Orientation of hexagonal prism gibbsite crystals; (B) well developed hexagonal gibbsite crystals (B-a) and their aggregation under high magnification; (C) well developed gibbsite crystals making loosely packed ball-like structures leaving voids; (D) deposition of gibbsite crystals on the surface of birnessite (D-a); (E) acicular crystals of goethite arranged into stars (E-a).

the soil solution (Peskley *et al.*, 2003). The individual gibbsite crystals were consistently ~5 µm in diameter and the thickness of individual crystals is ~0.2 µm (Figure 5B-a). Hsu (1989) reported that Al hydroxides

tend to grow intensively in the *X* and *Y* dimensions, with only limited growth in the *Z* direction. This is attributed to strong Al–OH–Al bonding within the layers and the relatively weak H bonding between layers.

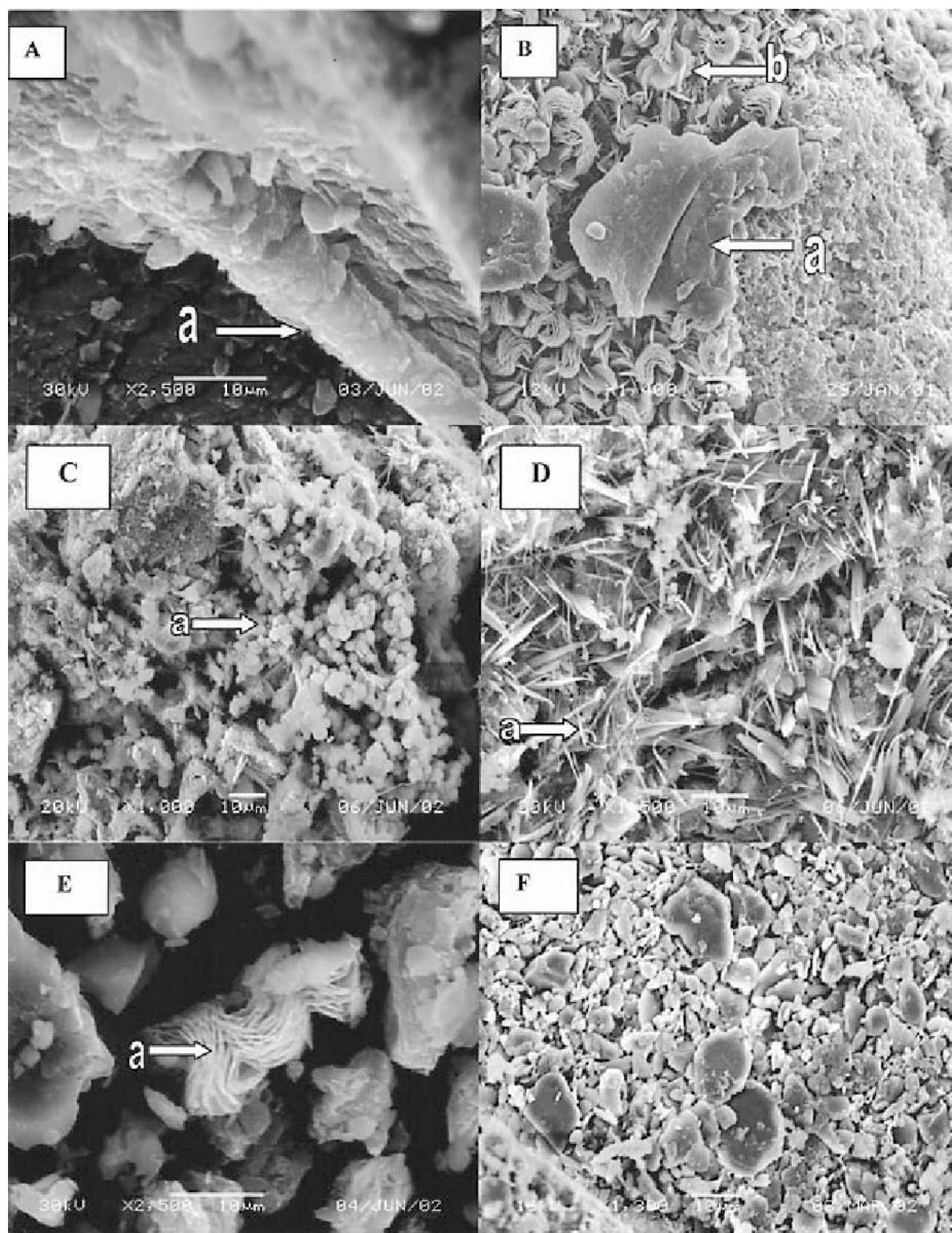


Figure 6. SEM images of untreated and SSDP-treated residues; (A) uneven kaolinite crystals make book like structures (A-a) of untreated samples; (B) irregular kaolinite crystals (B-a) associated with gibbsite (B-b) of untreated sample; (C) undissolved birnessite (C-a) after NaOH treatment; (D) undissolved goethite (D-a) after NaOH treatment; (E) Undissolved lithiophorite (E-a) after HAHC (25°C); (F) undissolved other silicate minerals after completely dissolving goethite in NaOH, HAHC and DCB treatments.

Silicate minerals: illite and kaolinite. Illite was proposed (Grim *et al.*, 1937) as a name for the 'mica occurring in argillaceous sediments'. It is considered a sedimentary mica commonly formed diagenetically in smectite clays. Brittle/soft Fe/Mn concretions collected from imperfectly drained, highly weathered soil originate from the Ryukyu limestone. Therefore, peaks appeared in the XRD analysis of the whole-soil sample at 1.00 nm, 0.50 nm and 0.334 nm, indicating the presence of illite, in spite of the treatments with NaOH, HAHC and DCB. The SEM observations (Figure 4F-a) also prove that weathered brittle/soft Fe/Mn concretions contain illite (secondary minerals) rather than a primary mica mineral. Detailed micromorphological information from illite minerals that are found in brittle/soft concretions is presented in Figure 4F-a. Irregular platy crystals of illite represent 'card-house stacking' (Figure 4F-a) and those crystals aggregate leaving voids.

Book-like structures of kaolinite are embedded inside silicate minerals (Figure 6A) of brittle/soft Fe/Mn concretions. The SEM images show that the crystal shapes are platy pseudohexagons with subhedral to euhedral outlines, and most of the crystals have smooth basal planes. Irregular kaolinite (Figure 6B-b) crystals are also closely associated with gibbsite crystals (Figure 6B-a).

Hexagonal crystals of soil kaolinite have been reported by numerous researchers (Dixon, 1999; Zbiku and Smart, 1998; Psyrillos *et al.*, 1999). Kaolinite pseudomorphs derived from primary phyllosilicates might have implications for the behavior of elements and the process of formation of kaolinite in weathering profiles (Jeong, 1998). The presence of gibbsite is indicative of intense weathering, and gibbsite followed by kaolinite in brittle/soft concretions indicates that weathering reached an extreme stage. This agrees with the findings of Phillips *et al.* (1998) and Islam *et al.* (2002).

Effectiveness of the reagents of sequential selective dissolution procedure

Electron micrographs of untreated silt-clay samples illustrate the micromorphology of kaolinite, gibbsite and other silicate minerals (Figure 6A,B). However, NaOH-treated samples clearly show the presence of goethite and birnessite minerals (Figure 6C,D) after kaolinite, gibbsite and unknown silicate minerals were dissolved. Moreover, sequential dissolution reagents of the HAHC (25°C) were able to dissolve birnessite but not lithiophorite (Figure 6E). Evidence of lithiophorite was not found by XRD or SEM in the HAHC (60°C)-treated samples, indicating that the lithiophorite was effectively dissolved by the HAHC at 60°C. The micromorphology of goethite was clear after the samples were treated with NaOH, due to dissolution of kaolinite and gibbsite minerals. Moreover, goethite completely disappeared after the DCB treatment (Figure 6F). The XRD results of

this study also proved that HAHC treatment was able to completely dissolve birnessite and lithiophorite at 25°C and 60°C, respectively, while the remaining goethite was not dissolved.

CONCLUSIONS

It is evident from the results that the selective dissolution sequence is able to differentiate between Mn, Fe and other phases and therefore helps in identification. The detailed micromorphology of these minerals illustrate that poorly developed birnessite crystals form globe-shaped aggregates and are closely associated with lithiophorite. Well developed, hexagonal gibbsite plates are clustered systematically in different directions to make foliated vermiciform structures. Pseudo-hexagonal plates of natural lithiophorite have produced thread-ball structures and acicular goethite crystals are arranged in star-shaped aggregates. The detailed micromorphology and mineral characteristics of Fe/Mn concretions in Okinawan soils may help with the interpretation of results from natural Fe/Mn minerals, obtained from various investigations.

ACKNOWLEDGMENTS

The authors wish to thank Prof. Hiroya Hayashi, Department of Bioscience and Biotechnology, Faculty of Agriculture, University of the Ryukyus, for the use of the scanning electron microscope. The first author is grateful to Dr U. P. de S. Waidynatha, the Chairman and the Directorate of the Coconut Research Board, Sri Lanka, for approving the sabbatical leave to conduct this study. Special thanks are also extended to Dr Lara Jeff (DHS-MCPD-RDB-RDPRS), MS 8304, PO Box 942732, Sacramento, CA 94234-7321, USA, for help in editing the manuscript. The authors wish to thank Mr Alexander Pereira De Barkker (PhD student, Brazil), Mr Tatsuya Nishi, Miss Kumiko Uehara and Yoshimi Shimabukuro for their assistance and kind cooperation.

REFERENCES

- Barbara, A.C., Steve, J.C., David, L.B. and Sandra, J.C. (1993) Fracture-lining manganese oxide minerals in Silicic tuff, Yucca Mountain, Nevada, U.S.A. *Chemical Geology*, **107**, 47–69.
- Burns, R.G. and Burns, V.M. (1977) Manganese oxides. Pp. 185–248 in: *Marine Manganese Nodules* (G.P. Glasby, editor). Elsevier, Amsterdam, The Netherlands.
- Chao, T.T. (1972) Selective dissolution of manganese oxides from soils and sediments with acidified hydroxylamine hydrochloride. *Soil Science Society of America Proceedings*, **36**, 764–768.
- Davey, B.G. (1978) Soil structure as revealed by scanning electron microscopy. Pp. 97–102 in: *Modification of Soil Structures* (W.W. Emerson, editor). John Wiley & Sons, New York.
- Dixon, J.B. (1999) Instruction in HRTEM through the useful example of goethite in soils. *Proceedings of the 11th International Clay Conference, Ottawa, Canada*, pp. 385–808.
- Dixon, J.B. (2002) *Soil Mineralogy: Recent Discoveries and their Implications*. Report of the Department of Soil and

- Crop Sciences, Texas A & M University, College Station, Texas, USA, pp. 1–4.
- Eswaran, H., Stoops, G. and Sys, C. (1977) The micro-morphology of gibbsite forms in soils. *Journal of Soil Science*, **28**, 136–143.
- Fendorf, S.E. and Zasoski, R.J. (1992) Chromium (III) oxidation by α -MnO₂. 1. Characterization. *Environmental Science Technology*, **26**, 79–85.
- Ford, R.G., Bertsch, P.M. and Seaman, J.C. (1997) Goethite morphologies investigated via X-ray diffraction of oriented samples. *Clays and Clay Minerals*, **45**, 769–772.
- Golden, D.C., Chen, C.C., Dixon, J.B. and Tokashiki, Y. (1988) Pseudomorphic replacement of manganese oxides by iron oxide minerals. *Geoderma*, **42**, 199–211.
- Golden, D.C., Dixon, J.B. and Kanehiro, Y. (1993) The manganese oxide minerals, lithiophorite in an Oxisol from Hawaii. *Australian Journal of Soil Research*, **31**, 51–66.
- Grim, R.E., Bray, R.H. and Bradley, W.F. (1937) The mica in argillaceous sediments. *American Mineralogist*, **22**, 813–829.
- Hsu, H.P. (1989) Aluminium hydroxides and oxyhydroxides. Pp. 331–378 in: *Minerals in Soil Environments* (J.B. Dixon and S.B. Weed, editors). Soil Science Society of America, Madison, Wisconsin.
- Islam, M.R., Stuart, R., Risto, A. and Vesa, P. (2002) Mineralogical changes during intense chemical weathering of sedimentary rocks in Bangladesh. *Journal of Asian Earth Sciences*, **20**, 889–901.
- Jackson, M.L. (1969) *Soil Chemical Analysis – Advanced Course*, 2nd edition. Published by the author, University of Wisconsin, Madison, Wisconsin.
- Jeong, G.Y. (1998) Vermicular kaolinite epitactic on primary phyllosilicates in the weathering profiles of anorthosite. *Clays and Clay Minerals*, **46**, 509–520.
- Lonsdale, P., Burns, V.M. and Fisk, M. (1980) Nodules of hydrothermal birnessite in the caldera of a young seamount. *Journal of Geology*, **88**, 611–618.
- McDaniel, P.A. and Buol, S.W. (1991) Manganese distributions in acid soils of the North Carolina Piedmont. *Soil Science Society of America Journal*, **55**, 152–158.
- McKenzie, R.M. (1989) Manganese oxides and hydroxides. Pp. 439–461 in: *Minerals and Soil Environment* (J.B. Dixon and S.B. Weed, editors). Soil Science Society of America, Madison, Wisconsin.
- Mehra, O.P. and Jackson, M.L. (1960) Iron oxide removal from soils and clays by dithionite citrate system buffered with sodium bicarbonate. *Clays and Clay Minerals*, **7**, 317–327.
- Min Zhang, M. and Karathanasis, A.D. (1997) Characterization of iron-manganese concretions in Kentucky Alfisols with perched water table. *Clays and Clay Minerals*, **45**, 428–439.
- Pauling, L. and Barclay, K. (1982) The crystal structure of lithiophorite. *American Mineralogist*, **67**, 817.
- Peskleway, C.D., Henderson, G.S. and Wicks, F.J. (2003) Dissolution of gibbsite: Direct observation using fluid cell atomic force microscopy. *American Mineralogist*, **88**, 8–26.
- Phillips, D.H., Ammons, J.T., Lee, S.Y. and Lietzke, D.A. (1998) Deep weathering of calcareous sedimentary rock and the redistribution of iron and manganese in soil and saprolite. *Soil Science*, **163**, 71–81.
- Post, J.E. (1999) Manganese oxide minerals: crystal structures and economic and environmental significance. *Proceedings of National Academy of Science of the United States of America*, **96**, 3447–3454.
- Post, J.E. and Appleman, D.E. (1994) Crystal-structure refinement of lithiophorite. *American Mineralogist*, **79**, 370–374.
- Psyrillos, A., Howe, J.H., Manning, D.A.C. and Burley, S.D. (1999) Geological controls on kaolin particle shape and consequences for mineral processing. *Clay Minerals*, **34**, 193–208.
- Ross, S.J., Franzmeier, D.P. and Roth, C.B. (1976) Mineralogy and chemistry of manganese oxides in some Indiana soils. *Soil Science Society of America Journal*, **40**, 137–143.
- Schwertmann, U. and Kampf, N. (1988) Properties of goethite and hematite in kaolinitic soils of southern and central Brazil. *Soil Science*, **139**, 344–350.
- Schwertmann, U. and Taylor, R.M. (1989) Iron Oxides. Pp. 379–438 in: *Minerals in Soil Environments* (J.B. Dixon and S.B. Weed, editors). Soil Science Society of America, Madison, Wisconsin.
- Sean, F., Andrew, R., Mei-Yin, L., Julian, G. and Gordon, P. (2000) Atomic modeling of gibbsite: surface structure and morphology. *Journal of Crystal Growth*, **209**, 159–166.
- Sweegers, C., van Enckevort, W.J.P., Meekes, H., Bennema, P., Hiralal, I.D.K. and Rijkeboer, A. (1999) The impact of twinning on the morphology of α -Al(OH)₃ crystals. *Journal of Crystal Growth*, **197**, 244–253.
- Tokashiki, Y., Dixon, J.B. and Golden, D.C. (1986) Manganese oxide analysis in soils by combined X-ray diffraction and selective dissolution methods. *Soil Science Society of America Journal*, **50**, 1079–1083.
- Tokashiki, Y., Kai, N., Henton, T., Shimo, M. and Vidhana Arachchi, L.P. (2003) A successive selective dissolution procedure for separation of birnessite, lithiophorite and goethite in manganese nodules. *Soil Science Society of America Journal*, **67**, 837–843.
- Usui, A. and Mita, N. (1995) Geochemistry and morphology of a modern buserite concretion from a hot spring in Hokkaido, Japan. *Clays and Clay Minerals*, **43**, 116–127.
- Uzochukwu, G.A. and Dixon, J.B. (1986) Manganese oxide minerals in nodules of two soils of Texas and Alabama. *Soil Science Society of America Journal*, **50**, 1358–1363.
- White, N.G. and Dixon, J.B. (1986) Iron manganese distribution in nodules from a young Texas vertisol. *Soil Science Society of America Journal*, **60**, 1254–1262.
- Yang, D.S. and Wang, M.K. (2003) Characterization and a fast method for synthesis of sub-micron lithiophorite. *Clays and Clay Minerals*, **51**, 96–101.
- Zbiku, M. and Smart, R.St.C. (1998) Nanomorphology of kaolinites: comparative SEM and TEM studies. *Clays and Clay Minerals*, **46**, 153–160.

(Received 10 June 2003; revised 23 February 2004;
Ms. 798; A.E. Helge Stanjek)